Eur. Phys. J. A **28**, 19–25 (2006)
DOI 10.1140/epja/i2005-10279-7

THE EUROPEAN PHYSICAL JOURNAL A

Variational approach to magnetic bands in ^{82}Rb

A. Petrovici[1,2,a], K.W. Schmid[2], O. Radu[1], and A. Faessler[2]

[1] National Institute for Physics and Nuclear Engineering, R-76900 Bucharest, Romania
[2] Institut für Theoretische Physik, Universität Tübingen, D-72076 Tübingen, Germany

Received: 20 December 2005 / Revised version: 16 March 2006 /
Published online: 26 May 2006 –
Communicated by A. Molinari

Abstract. The *complex* Excited Vampir approach was applied to the description of the recently identified magnetic cascade of negative-parity states in the odd-odd ^{82}Rb nucleus. Strong $M1$, $\Delta I = 1$ transitions as well as rather weak crossover $B(E2)$ strengths are obtained in agreement with the available data. The decrease of the $B(M1)$ strengths with increasing spin is revealed by the calculations. A strong mixing of differently deformed states at the highest calculated spins is responsible for the trend of the $B(M1; \Delta I = 1)$ and $B(E2; \Delta I = 2)$ strengths.

PACS. 21.10.-k Properties of nuclei; nuclear energy levels – 21.60.-n Nuclear structure models and methods – 27.50.+e $59 \leq A \leq 89$

1 Introduction

The cascading sequences of magnetic dipole transitions established in the proton-rich Pb isotopes are well described within the framework of the Tilted Axis Cranking (TAC) approach [1]. The TAC results indicate that the angular momentum along the dipole bands is generated mainly by a reorientation of few proton particles (holes) and neutron holes (particles) in high-j orbitals into the direction of the total angular momentum. The most important signature of such a magnetic rotational (or shears) band is a sharp decrease in the $B(M1)$ values with increasing angular momentum. Shell model studies of shears bands in light Pb nuclei [2] suggested that a certain polarizability of the low-j core is important to stabilize these bands.

These type of bands were predicted to appear also in the $A = 140$, $A = 110$, and $A = 80$ mass regions [3]. Studying the existence of magnetic rotational bands in the odd-A Rb isotopes, Amita *et al.* [4] concluded that shears mechanism seems to be valid in the $\Delta I = 1$ bands, although it is not the only mechanism responsible for the generation of angular momentum, since they are situated at the beginning of the transitional region between magnetic and conventional collective regions. It is worthwhile to mention that our previous investigations concerning the structure of odd-odd nuclei in the $A = 70$–80 mass region within the Excited Vampir or Excited Fed Vampir variational approaches revealed the appearance of strong $M1$, $\Delta I = 1$ transitions at intermediate and high spins connecting the positive (negative) parity states of even- and odd-spin bands [5–7]. The longest sequence of strong $M1$ transitions was found to connect the states of one pair of strongly deformed even- and odd-spin bands calculated in ^{78}Rb [6].

Recent experimental results on high-spin states in the nuclei ^{82}Rb and ^{84}Rb indicate the presence of regular magnetic dipole bands including strong $M1$ and relatively weak $E2$ transitions [8–10]. These bands have been successfully described within the tilted axis cranking model on the basis of the four-quasiparticle configuration $\pi(fp)\pi(g_{9/2}^2)\nu(g_{9/2})$. Shell model calculations as well as relativistic mean-field descriptions for the shears band mechanism in ^{84}Rb have been recently accomplished [10,11].

The aim of the present paper is to get a microscopic description of the magnetic sequence of negative-parity states along with the relatively weak $E2$ crossover transitions identified in ^{82}Rb [8–10] using the *complex* Excited Vampir approach. Models based on the variational approaches of the Vampir family have been successfully applied for the description of a variety of nuclear-structure phenomena in the $A = 70$–80 nuclei. Spectroscopic investigations of even-even and odd-odd systems demonstrated that this mass region is very rich in nuclear-structure aspects. Coexistence of a variety of nuclear shapes from weakly to largely deformed oblate and prolate configurations has been found. The *complex* Excited Vampir approach is able to describe the oblate-prolate coexistence and mixing, the variation of the deformation with mass number, increasing spin, as well as excitation energy. As we shall see these Vampir approaches, which allow the use

[a] e-mail: spetro@ifin.nipne.ro

of rather large model spaces and of general two-body interactions, provide also a nice interpretation of the properties of the sequences of strong dipole transitions found in the odd-odd Rb nuclei. Our previous investigations on microscopic aspects of coexistence phenomena in the $A = 70$–80 nuclei indicated the presence of a strong competition between particular configurations based on large and small oblate and prolate quadrupole deformations. Furthermore, it was demonstrated that the neutron and proton alignments with increasing angular momentum may occur simultaneously in these nuclei. On the other hand, the theoretical results suggest that certain properties of these nuclei are extremely sensitive to small variations of particular parts of the effective Hamiltonian [7]. Thus, our results indicate that the coexistence and mixing of differently deformed configurations depend on the strengths of the neutron-proton $T = 0$ matrix elements involving nucleons occupying the $0f_{5/2}(0f_{7/2})$ and $0g_{9/2}$ single-particle orbits.

Since most of our predictions concerning the structure of even-even and odd-odd nuclei in this mass region have been confirmed experimentally, we thought it worthwhile to apply the same methods to get a microscopic description of the properties of the identified magnetic cascade in the ^{82}Rb nucleus. We shall briefly describe the *complex* Excited Vampir variational procedure and define the effective Hamiltonian in the next section. In sect. 3 we shall discuss the results on magnetic band structures in the ^{82}Rb nucleus. Finally, we shall present some conclusions in sect. 4.

2 Theoretical framework

We calculated negative-parity states up to spin 18^- in ^{82}Rb. First, the Vampir solutions, representing the optimal mean-field description of the yrast states by single symmetry-projected Hartree-Fock-Bogoliubov (HFB) determinants, were obtained. Then, the Excited Vampir approach was used to construct additional excited states by independent variational calculations. Finally, for each considered spin the residual interaction between the various orthogonal configurations was diagonalized.

We define the model space and the effective Hamiltonian as in our earlier calculations for nuclei in the $A = 70$–80 mass region [7]: a ^{40}Ca core is used and the valence space consists out of the $1p_{1/2}$, $1p_{3/2}$, $0f_{5/2}$, $0f_{7/2}$, $1d_{5/2}$ and $0g_{9/2}$ oscillator orbits for both protons and neutrons. For the corresponding single-particle energies we take (in units of the oscillator energy $\hbar\omega = 41.2A^{-1/3}$) 0.040, −0.270, 0.300, −0.560, 0.157 and 0.029 for the proton, and −0.070, −0.332, 0.130, −0.690, 0.079 and −0.043 for the neutron levels, respectively. The effective two-body interaction is a renormalized nuclear matter G-matrix based on the Bonn One-Boson-Exchange potential (Bonn A). The G-matrix is modified by three short-range (0.707 fm) Gaussians for the isospin $T = 1$ proton-proton, neutron-neutron and neutron-proton matrix elements with strengths of −40, −30, and −35 MeV, respectively. The isoscalar spin 0 and 1 particle-particle matrix elements are enhanced by an additional Gaussian with the same range and the strength of −180 MeV. In addition, the interaction contains monopole shifts of −325 keV (−375 keV) for all the diagonal isospin $T = 0$ matrix elements of the form $\langle 0g_{9/2}0f; IT = 0|\hat{G}|0g_{9/2}0f; IT = 0\rangle$ with $0f$ denoting either the $0f_{5/2}$ or the $0f_{7/2}$ orbit, and −500 keV for $\langle 1p1d_{5/2}; IT = 0|\hat{G}|1p1d_{5/2}; IT = 0\rangle$, where $1p$ denotes either the $1p_{1/2}$ or the $1p_{3/2}$ orbit. The corresponding Hamiltonian is denoted by H_1 (H_2) in the following.

3 Results and discussion

Since particular properties of the $A = 70$–80 nuclei depend sensitively on the strengths of the above-mentioned monopole shifts involving neutrons and protons occupying the $0f$ and $0g_{9/2}$ orbitals two types of calculations have been performed using either −325 keV (Hamiltonian H_1) or −375 keV (Hamiltonian H_2).

Using the Hamiltonian H_1 the negative-parity states up to spin 18^- have been calculated including in the many-nucleon basis the lowest 8 up to 18 Excited Vampir configurations depending on the level density specific for each considered spin. Different types of structures have been obtained: states dominated by spherical configurations, almost pure oblate-deformed states, states based on a strong mixing of configurations characterized by smaller or larger quadrupole deformation in the intrinsic system.

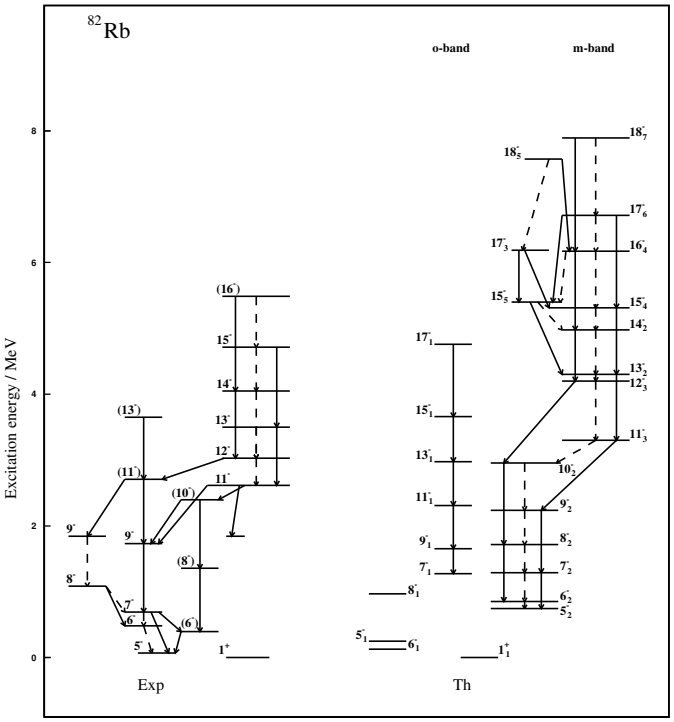

Fig. 1. The theoretical spectrum of ^{82}Rb for negative-parity states calculated within the *complex* Excited Vampir approximation using the H_1 Hamiltonian is compared to the experimental results [10].

Table 1. The amount of mixing for some states of ^{82}Rb presented in figs. 1 and 2.

	H_1		H_2			
	m-band		m^*-band		m-band	
I^π [$\hbar$]	o-mixing	p-mixing	o-mixing	p-mixing	o-mixing	p-mixing
5^-		98%		98%		
6^-		99%		83(12)%		
7^-		98%		97%		
8^-		99%		97%		
9^-		99%		94%		96(3)%
10^-		99%		95%	12(8)(4)%	57(4)(4)%
11^-		97%	3%	87(6)%		90(7)%
12^-	21(7)(3)%	60(7)%	23(10)(7)(3)	47(4)%	4%	59(15)(13)%
13^-		95%	23(11)(4)(3)%	50(4)%	11%	66(19)%
14^-		88(9)%	30(8)(7)(4)%	18(11)(5)(3)(3)%	6%	56(27)(3)%
15^-	29%	66%	44(9)(8)%	27(3)(3)%	5(3)%	62(21)%
16^-	3%	88(5)(4)%			33%	23(30)(7)%
17^-	9(6)%	63(8)(6)%			7(7)(5)(4)%	68(3)%
18^-	12%	59(16)(6)%			8%	54(23)(3)%

Searching for $\Delta I = 1$ cascades of states connected by strong $B(M1)$ transitions as well as significant $B(E2, \Delta I = 2)$ strengths, like the one identified experimentally, we linked the states in bands. In fig. 1 we present the calculated lowest few states which are based on spherical configurations, as well as the lowest collective band which was found to have oblate character (o-band).

The excited even- and odd-spin negative-parity states are characterized by a high level density for spins above 11^-. The most probable candidate for the experimental "magnetic sequence of states" are the states linked in the band labeled m-band in fig. 1. Up to spin 11^- the states of this band are dominated by a single prolate-deformed configuration as is illustrated in table 1. This table presents the amount of mixing of differently deformed symmetry-projected configurations underlying the structure of the discussed states representing at least 3% in amplitude. The higher-spin states of this band display a variable mixing involving besides the main configuration other prolate- or oblate-deformed ones characterized by moderate or small quadrupole deformation in the intrinsic system.

The $B(E2; I \to I-2)$ values for the calculated bands presented in fig. 1 as well as the available data are given in table 2. As effective charges $e_p = 1.25$ and $e_n = 0.25$ have been used. Since the 12^-, 15^-, 17^- and 18^- states of the m-band are strongly mixed, each state is decaying by at least two significant $E2, \Delta I = 2$ branches. The fragmentation of the $B(E2)$ strengths explains the irregular behaviour of the $B(E2)$ values connecting the $\Delta I = 2$ states inside the m-band. In addition, part of the feeding of the states belonging to the m-band is produced by significant $M1$ and $E2$ transitions from the decay of some states closely lying in energy with respect to the ones building the band as is the case for the 15^-, 17^- and 18^- states presented on the left side of the m-band in fig. 1. The strength for the secondary $E2$ branch feeding the 13^-_2 state amounts to $B(E2; 15^-_5 \to 13^-_2) = 155\ e^2\text{fm}^4$, while

Table 2. $B(E2; I \to I-2)$ values (in $e^2\text{fm}^4$) for some states of the nucleus ^{82}Rb presented in figs. 1 and 2.

		H_1		H_2		
I^π [$\hbar$]	Exp	o-band	m-band	o-band	m^*-band	m-band
7^-			868		815	
8^-			1232		668	
9^-		666	896	562	824	
10^-			897		828	
11^-		610	826	516	828	840
12^-			238		490	196
13^-	384^{+131}_{-106}	545	807	424	273	583
14^-	511^{+193}_{-129}		473		101	487
15^-	>110	534	634	436	205	618
16^-			628			349
17^-		428	191	330		302
18^-			277			66

Table 3. $B(M1; I \to I-1)$ values (in μ_N^2) for some states of the nucleus ^{82}Rb presented in figs. 1 and 2.

		H_1	H_2	
I^π [$\hbar$]	Exp	m-band	m^*-band	m-band
7^-		2.03	1.66	
8^-		1.43	1.36	
9^-		2.03	2.09	
10^-		1.00	1.00	0.48
11^-		1.50	1.99	1.13
12^-	$1.24^{+0.37}_{-0.24}$	0.35	0.35	0.45
13^-	$0.77^{+0.20}_{-0.13}$	1.21	0.86	0.86
14^-	$0.74^{+0.22}_{-0.14}$	0.55	0.06	0.46
15^-	>0.11	0.62	0.26	1.04
16^-		0.52		0.40
17^-		0.87		0.07
18^-		0.63		0.33

the main $E2$ branch feeding the 15_5^- state is $B(E2; 17_6^- \to 15_5^-) = 414\ e^2\text{fm}^4$. This picture corresponds to the structure of the wave functions illustrated in table 1, which reveals a smaller contribution of the projected configuration dominating the structure of the states linked in the m-band with increasing spin. In fact the main component of the states presented on the left side of the band is an oblate-deformed configuration representing almost 70% of the total wave function.

In table 3 the results concerning the strengths of the $M1$ transitions inside the m-band together with the experimental available information are presented. Here the free values for the g-factors have been used. Significant strengths have been obtained for the secondary $M1$ branches indicated in fig. 1: $B(M1; 15_5^- \to 14_2^-) = 0.35\mu_N^2$, $B(M1; 16_4^- \to 15_5^-) = 0.24\mu_N^2$, $B(M1; 18_5^- \to 17_3^-) = 0.29\mu_N^2$, but only $B(M1; 17_3^- \to 16_4^-) = 0.03\mu_N^2$ for the closely lying states 17_3^- and 16_4^-.

In order to investigate the influence of the monopole shifts as well as the the possible appearance of other "magnetic structures" we accomplished a second type of calculations using the H_2 Hamiltonian and increasing drastically the dimension of the Excited Vampir basis for each investigated spin. The results presented in fig. 2 have been obtained using at least 30 symmetry projected configurations for the states of spin higher than 9^-. Besides the analogue of the m-band obtained using the H_1 Hamiltonian a new band (m^*-band) characterized by few significant $M1$ transitions and relatively weak $B(E2)$ strengths at intermediate spins was found as is illustrated in fig. 2.

Comparing the structure of the m-band states obtained using the two types of calculations we can see from table 1 that the mixing manifested by the states with spin higher than 11^- is much stronger for the second series of calculations involving many more Excited Vampir configurations. The mixing is even stronger for the m^*-band starting with spin 12^-. The agreement of the calculated $B(E2, \Delta I = 2)$ values characterizing the m-band with the available data is rather good, while for the m^*-band weaker strengths have been obtained. Again, due to

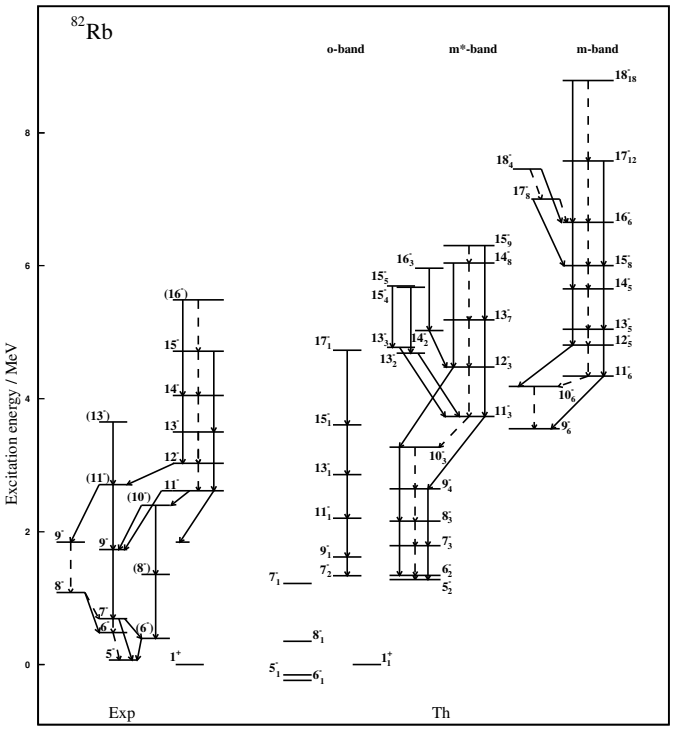

Fig. 2. The same as in fig. 1, but for the H_2 Hamiltonian.

the high density of states obtained for spins $I^\pi \geq 12^-$, each state is decaying and also fed by many significant $B(E2, \Delta I = 2)$ branches. This aspect is illustrated for the highest calculated spins presenting in fig. 2 an alternative way to continue the m-band above spin 16^-. For the states plotted on the left side of the m-band we obtained $B(E2; 17_8^- \to 15_8^-) = 214\ e^2\text{fm}^4$, and $B(E2; 18_4^- \to 16_6^-) = 143\ e^2\text{fm}^4$. For this competing branch the calculated $M1$ strengths are $B(M1; 17_8^- \to 16_6^-) = 0.75\mu_N^2$, and $B(M1; 18_4^- \to 17_8^-) = 0.15\mu_N^2$. A competing $E2$ feeding for the 11^- and 12^- states of the m^*-band is represented by the states plotted on the left side of the band.

The spectroscopic quadrupole moments of the states building the m-sequences presented in figs. 1 and 2 are given in table 4. The corresponding values reveal the strong mixing of configurations having different oblate and prolate deformations in the intrinsec system underlying the structure of the high-spin states belonging to these bands. The trend manifested in the Q_2^{sp} values for the highest calculated spins corroborated with the behaviour of the $B(E2, \Delta I = 2)$ values inside the m-band as well as the structure of the corresponding wave functions presented in table 1 for both types of calculations suggests the decrease of deformation with increasing spin.

The results presented in table 3 for the $B(M1, \Delta I = 1)$ strengths characterizing the m-band show a reasonable agreement with the available data. For the second type of calculations one obtains the required decrease of the $B(M1)$ values with increasing spin up to the highest calculated members included in the m-band. The calculated transition strengths indicate at intermediate spins a staggering difficult to compare with the present available data

Table 4. Spectroscopic quadrupole moments Q_2^{sp} (in $e$fm^2) of some states of ^{82}Rb presented in figs. 1 and 2.

	H_1	H_2	
I^π [$\hbar$]	m-band	m^*-band	m-band
5^-	-64.02	-60.11	
6^-	-66.11	-52.57	
7^-	-65.16	-62.39	
8^-	-68.36	-62.86	
9^-	-67.42	-59.30	-67.15
10^-	-67.28	-63.39	-35.39
11^-	-63.19	-54.69	-64.68
12^-	-26.57	-1.24	-58.23
13^-	-63.63	-4.66	-48.84
14^-	-67.43	5.18	-51.62
15^-	-26.80	10.82	-45.50
16^-	-65.59		-22.05
17^-	-37.80		-37.60
18^-	-36.58		-37.63

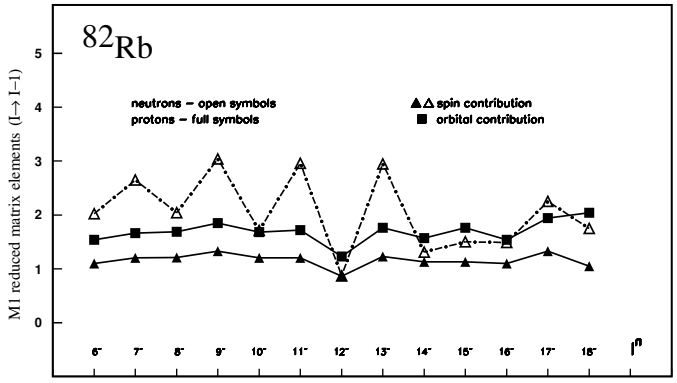

Fig. 3. The $M1$ reduced matrix elements (in relative units) for $I \to I-1$ transitions connecting the states of the m-band calculated using the H_1 Hamiltonian.

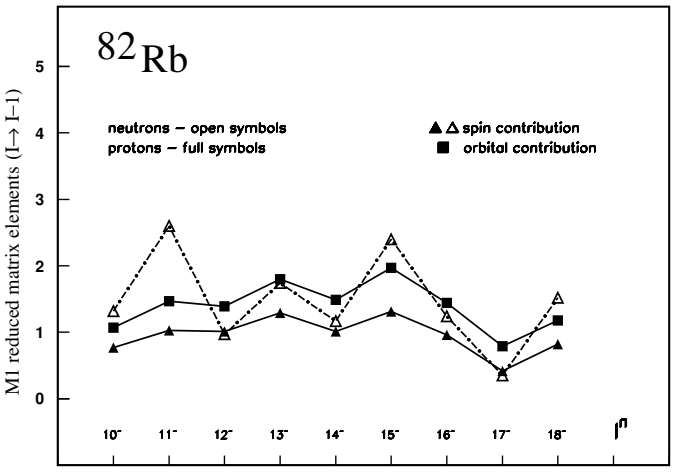

Fig. 4. The same as in fig. 3 for the H_2 Hamiltonian.

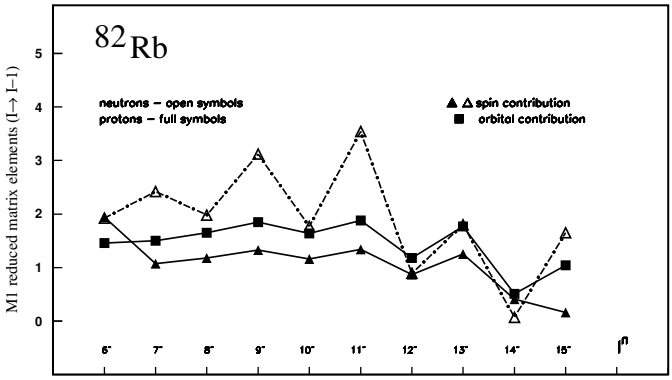

Fig. 5. The same as in fig. 4 for the calculated states of the m^*-band.

due to the somewhat large experimental errors. The level spacings are also more regular than the ones obtained in the first calculations indicating the importance of increasing the dimension of the Excited Vampir basis. The m^*-band which is very regular up to spin 14^- cannot be continued above spin 15^- with the same type of structure.

The orbital and spin contribution to the $B(M1; \Delta I = 1)$ strengths of the m-bands for the two types of calculations are presented in figs. 3 and 4. Both types of proton contributions (orbital and spin) are determined by rearrangements of the particles occupying the $0g_{9/2}$ orbital. The neutron contribution is determined essentially by particles occupying the $1p_{3/2}$ and $1p_{1/2}$ orbitals. It should be mentioned that the smaller contributions for the decay of the even-spin states are mainly produced by cancellations among these type of matrix elements. On the proton side the variations observed in both orbital and spin contributions are determined only by the particles occupying the $g_{9/2}$ orbital. The results presented in figs. 3 and 4 indicate that all three types of contributions are decreasing for the highest calculated spins. A similar behaviour is manifested in fig. 5 for the m^*-band.

The occupation of the neutron orbitals contributing to the $M1$ matrix elements is almost constant for both $1p_{1/2}$ (around 0.6 particles) and $1p_{3/2}$ (around 2.5 particles) spherical states for m-bands as well as for m^*-bands. The occupation of the neutron $g_{9/2}$ orbital is almost constant around 7.8 particles. Concerning the proton $g_{9/2}$ orbital a variation in between 3.1 and 3.8 particles is obtained for the m-bands, while for band m^*-band the occupation is varying in between 4.2 for spin 10^- and 4.5 for the 15^- state.

The analysis of the mixing of different configurations with increasing spin and the variation of the neutron and proton contributions to the total $M1$ strength for different spins indicates that besides the main component of the wave function other smaller components influence the decreasing trend with increasing spin for the calculated $B(M1)$ values presented in table 3.

In figs. 6 and 7 we present the alignment plot for the m-band using the H_1 Hamiltonian and for the m^*-band and m-band for H_2, respectively. Both types of calculations indicate strong alignment for the $g_{9/2}$ protons, but slow and weak alignment for the $g_{9/2}$ neutrons.

In fig. 8 we present the angular-momentum contribution of the particles occupying the $g_{9/2}$ orbital as percentage of the total spin for the calculations using the

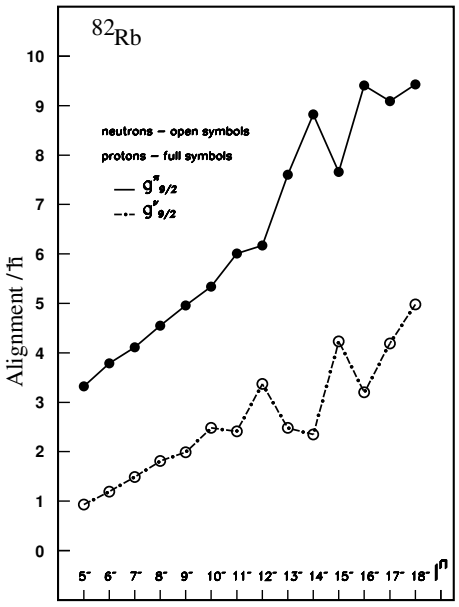

Fig. 6. The alignment plot for the m-band calculated in ^{82}Rb using the H_1 Hamiltonian.

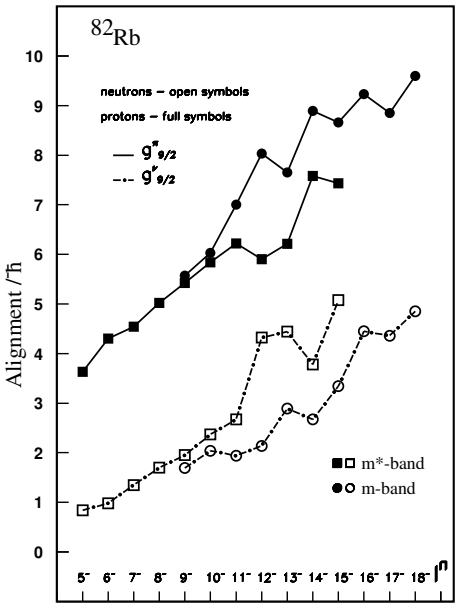

Fig. 7. The alignment plot for some of the calculated bands in ^{82}Rb using the H_2 Hamiltonian.

H_2 Hamiltonian. The plot illustrates the decrease of the contribution from protons occupying the $g_{9/2}$ orbital with increasing spin.

More experimental information is required in order establish the characteristic features of the possible magnetic bands predicted to appear in the $A = 80$ nuclei in order to improve the effective interaction and to distinguish between different types of magnetic cascades appearing in odd-odd and odd Rb isotopes.

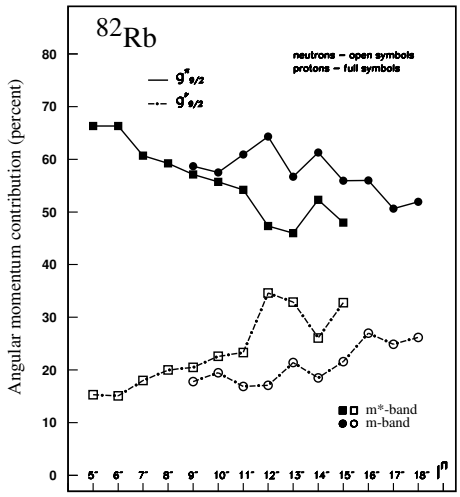

Fig. 8. The percentage contribution of the particles occupying the $g_{9/2}$ orbital to the total angular momentum for selected states in ^{82}Rb calculated using the H_2 Hamiltonian.

4 Conclusions

The *complex* Excited Vampir approach was applied to the description of the recently discovered magnetic cascade of negative-parity states in ^{82}Rb. Strong $M1$ $\Delta I = 1$ transitions as well as rather weak $E2$ crossover transitions connecting negative-parity states have been obtained in reasonable agreement with the available data. The main property of the magnetic rotational bands is the decrease of the $B(M1)$ strength with increasing spin. This can be explained by the increased mixing of configurations underlying the structure of the states building the bands. Consequently, very large many-nucleon model spaces are required in order to determine the structure of the corresponding wave functions. An improved effective interaction could be determined if more experimental information were available. Extensive calculations for ^{84}Rb nucleus will be accomplished in order to complete the Excited Vampir description of the mechanism responsible for the magnetic rotation in this mass region.

References

1. S. Frauendorf, Nucl. Phys. A **557**, 259c (1993).
2. S. Frauendorf, J. Reif, G. Winter, Nucl. Phys. A **601**, 41 (1996).
3. S. Frauendorf, Z. Phys. A **358**, 163 (1997).
4. Amita, A.K. Jain, V.I. Dimitrov, S.G. Frauendorf, Phys. Rev. C **64**, 034308 (2001).
5. A. Petrovici, K.W. Schmid, A. Faessler, D. Pantelica, F. Negoita, B.R.S. Babu, A.V. Ramayya, J.H. Hamilton, J. Kormicki, L. Chaturvedi, W.C. Ma, S.J. Zhu, N.R. Johnson, I.Y. Lee, C. Baktash, F.K. McGowan, M.L. Halbert, M. Riley, J.D. Cole, Phys. Rev. C **53**, 2134 (1996).
6. A. Petrovici, K.W. Schmid, A. Faessler, Z. Phys. A **359**, 19 (1997).
7. A. Petrovici, K.W. Schmid, A. Faessler, J.H. Hamilton, A.V. Ramayya, Prog. Part. Nucl. Phys. **43**, 485 (1999).

8. J. Döring, D. Ulrich, G.D. Johns, M.A. Riley, S.L. Tabor, Phys. Rev. C **59**, 71 (1999).
9. H. Schnare, R. Schwengner, S. Frauendorf, F. Dönau, L. Käubler, H. Prade, A. Jungclaus, K.P. Lieb, C. Lingk, S. Skoda, J. Eberth, G. de Angelis, A. Gadea, E. Farnea, D.R. Napoli, C.A. Ur, G. Lo Bianco, Phys. Rev. Lett. **82**, 4408 (1999).
10. R. Schwengner, G. Rainovski, H. Schnare, A. Wagner, F. Dönau, A. Jungclaus, M. Hausmann, O. Iordanov, K.P. Lieb, D.R. Napoli, G. de Angelis, M. Axiotis, N. Marginean, F. Brandolini, C. Rossi Alvarez, Phys. Rev. C **66**, 024310 (2002).
11. H. Madokoro, J. Meng, M. Matsuzaki, S. Yamaji, Phys. Rev. C **62**, 061301(R) (2000).